

Flexoelectricity causes surface piezoelectric-like effects in dielectrics

H. Mohammadi^{a,b}, F. Greco^{a,c,*}, D. Codony^{a,d}, I. Arias^{a,b}

^aLaboratori de Càlcul Numèric (LaCàN), Universitat Politècnica de Catalunya (UPC), Campus Nord UPC-C2, E-08034 Barcelona, Spain

^bCentre Internacional de Mètodes Numèrics en Enginyeria (CIMNE), 08034 Barcelona, Spain

^cDepartment of Mining, Industrial and ICT Engineering, Universitat Politècnica de Catalunya (UPC), Campus Manresa, E-08242 Manresa, Spain

^dCollege of Engineering, Georgia Institute of Technology, Atlanta, Georgia 30332, USA

Abstract

In this paper we study the surface effects that bulk flexoelectric models in finite samples exhibit. We first show that when the body is infinite, flexoelectric materials do not exhibit electromechanical response under homogeneous loading. However, when the size of the body is finite, due to the symmetry-breaking nature of surfaces, homogeneous loading (mechanical or electrical) can cause an electromechanical response near the surfaces. We obtain closed-form solutions for finite samples under different electromechanical loading conditions, and show that the electromechanical response caused by the bulk flexoelectric effect is reminiscent of surface piezoelectricity, causing boundary layers in certain components of the strains and/or electric fields near the free surfaces.

Keywords: Flexoelectricity, Surface effects, Finite size, Continuum.

1. Introduction

Flexoelectricity, a linear couplings between strain gradient and electric field (direct flexoelectricity) or between electric field gradient and strain (converse flexoelectricity), is present in all dielectric materials, including crystals, polymers, biomaterials, liquid crystals, etc. (Zubko et al., 2013, Nguyen et al., 2013, Ahmadpoor and Sharma, 2015, Wang et al., 2019). These couplings, which were first predicted theoretically (Mashkevich and Tolpygo, 1957) have since been confirmed experimentally. Bursian and Zaikovskii (1968) demonstrated beam bending of non-piezoelectric thin cantilever beams under applied electric bias in closed circuit, an evidence of inverse flexoelectricity producing non-homogeneous deformations in response to an applied homogeneous electric field. This effect has been later used in proof-of-concept flexoelectric MEMS (Bhaskar et al., 2016). Ma and Cross (2001, 2002) and Cross (2006) conducted a series of experiments showing electric fields emerging in cantilever nanobeams under bending and nanopryamids under compression, a testament of the direct flexoelectric effect.

The flexoelectric response induced by mechanical gradients has been shown to be strong enough to: (i) switch polarization in ferroelectrics, which opens avenues for mechanical writing of ferroelectric memories without any electrical bias (Lu et al., 2012), (ii) change the conductivity of LAO/STO interfaces by purely mechanical means, which can find application in transistors (Sharma et al., 2015), and (iii) provide a charge separation mechanism in non-centrosymmetric materials for photovoltaic applications (Yang et al., 2018). Finally, deformation under inhomogeneous electric fields due to converse flexoelectricity has been observed in Piezoresponse Force Microscopy (PFM) (Abdollahi et al., 2019). All these settings have been successfully modeled with a self-consistent two-way coupled electromechanical continuum framework, demonstrating the ability of the model to capture flexoelectric physics (Abdollahi et al., 2014, 2015, Codony et al., 2021, Abdollahi et al., 2019).

In all three flexoelectric mechanisms, the actuating field, namely a mechanical gradient (direct), an electric field (inverse) and an electric field gradient (converse) are polar in nature and thus able by themselves to break material centro-symmetry. This is not expected to happen under homogeneous strain (c.f. Fig. 1a). Indeed, the self-consistent

*Corresponding author

Email address: francesco.greco@upc.edu (F. Greco)

simulation of a non-piezoelectric dielectric square sample with generalized periodic boundaries (Barceló-Mercader et al., 2022, Barceló-Mercader et al., 2024a), i.e. representing an infinite medium, under uniform compression shows no flexoelectric response as expected (Fig. 1b). Interestingly, simulations in finite samples for all three models in Section 2 exhibit a boundary layer in the electric potential or the strain, which vanishes in the bulk as expected (Fig. 1c). This boundary layer emerges naturally from the model in the presence of a free surface. Intuitively, this localized electric response can be viewed as the piezoelectric-like response of a thin layer of material close to the free surface. It is thus reminiscent of surface piezoelectricity. This effect manifests itself in finite samples as an emerging thin piezoelectric boundary layer resulting from symmetry loss at the surface (Zubko et al., 2013).

Regardless of the intrinsic symmetry of the bulk material, the presence of a free surface breaks the symmetry by surface relaxation and induces the emergence of a thin layer of non-centrosymmetric material with piezoelectric-like behavior. Surface piezoelectricity has been modeled as a zero-thickness layer of piezoelectric material, in the spirit of Tagantsev and Yurkov (2012), Yudin and Tagantsev (2013), Yurkov and Tagantsev (2016). However, it is known that surface relaxation can be described by strain gradient elasticity (Danescu, 2012). Similarly, here a piezoelectric-like boundary layer emerges naturally from the rich continuum model, without a specific ad-hoc model for surface piezoelectricity. Similar to the boundary layers in strain gradient elasticity models (Lam et al., 2003, Shu et al., 1999, SHODJA et al., 2012), the observed boundary layers present an exponential growth near the surfaces, and their width is directly related to the length scale parameters of the inherent higher-order physics.

An in-depth understanding of the inherent surface effects of flexoelectric models is essential from modeling, computational, and physical perspectives. From the modeling side, the emergence of boundary layers from surface relaxation in the flexoelectric models needs to be taken into account when incorporating ad-hoc surface piezoelectricity models such as the zero-thickness piezoelectric surface layer as done in Dai et al. (2011) and Pan et al. (2011). Furthermore, a rigorous characterization of the boundary layers provides an opportunity to model surface effects resulting from surface relaxation as an emergent property. Obviously, surface effects resulting from physical or chemical surface specificity cannot be captured by the present rich continuum models. On the computational side (Codony et al., 2019, Yvonnet and Liu, 2017), the inherent surface effects of the flexoelectric models can cause steep boundary layers resulting in numerical instabilities if the computational mesh is not sufficiently fine. Quantitative knowledge of the inherent surface effects of the flexoelectric models can be a useful guide for careful consideration of the mesh size and/or regularization parameters. Finally, the detailed study of specific boundary value problems based on the rich continuum models can provide further insights on the physics of the free surface effects.

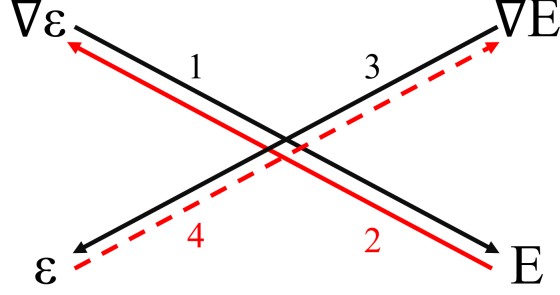
In the following sections, we present a theoretical exploration and characterization of the observed boundary layers. We first study two examples in which a homogeneous electric field or strain causes surface effects in a thin flexoelectric film. As an additional example, we then explore the uniform bending of a flexoelectric beam, showing that it exhibits surface effects that could be well-explained with the similarity to those seen due to the application of homogeneous strain.

2. Methodology

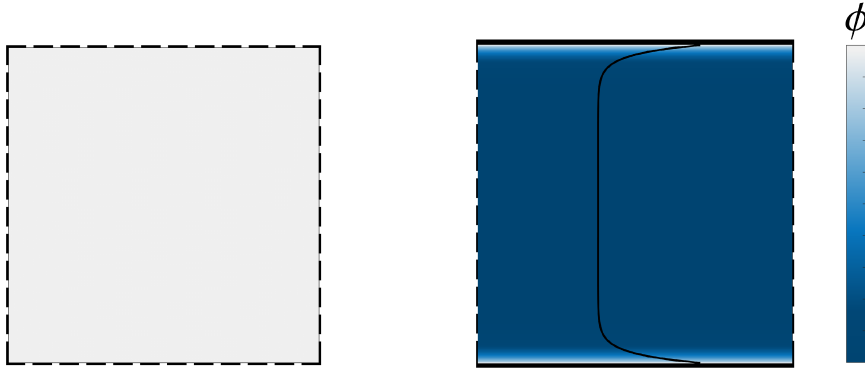
We consider a general form of flexoelectric coupling from which different forms such as direct, converse, and Lifshitz-invariant flexoelectric models (Codony et al., 2021) can be derived. In the limit of infinitesimal deformations, the electromechanical enthalpy density can be written in terms of strains ε_{ij} , electric fields E_l , and their gradients as:

$$\mathcal{H}(\varepsilon_{ij}, \varepsilon_{ijk}, E_l, E_{l,m}) = \frac{1}{2} \mathbf{C}_{ijkl} \varepsilon_{ij} \varepsilon_{kl} + \frac{1}{2} h_{ijklmn} \varepsilon_{ijk} \varepsilon_{lm,n} + \zeta \mu_{lijk} \varepsilon_{ij} E_{l,k} - (1 - \zeta) \mu_{lijk} \varepsilon_{ijk} E_l - \frac{1}{2} \kappa_{lm} E_l E_m - \frac{1}{2} M_{ijkl} E_{i,j} E_{k,l}, \quad (1)$$

where $\zeta = 0$ is related to the direct model, $\zeta = 1$ is related to the converse model, and $\zeta = 0.5$ is related to the Lifshitz-invariant model. In Eq. (1), \mathbf{C} is the elasticity tensor, \mathbf{h} is the strain gradient elasticity tensor, $\boldsymbol{\mu}$ is the flexoelectricity tensor, $\boldsymbol{\kappa}$ is the dielectricity tensor, and \mathbf{M} is the gradient dielectricity tensor. The material tensors are defined in Appendix A. The constitutive equations are:



(a) Four-way coupling in the continuum models of flexoelectricity, namely (1) direct flexoelectricity, (2) inverse flexoelectricity, (3) converse flexoelectricity, (4) inverse-converse flexoelectricity. The first three phenomena have been confirmed experimentally, while the fourth one has not yet been observed.



(b) Horizontal (x) compression of an infinite flexoelectric body (periodic in x and y directions) does not induce any electric response, as symmetry is not broken with compression.

(c) Horizontal (x) compression of an infinite flexoelectric film (periodic in x but finite in y direction) induces an electric response close to the free top and bottom boundaries, as surfaces are sources of symmetry-breaking.

Figure 1: Flexoelectric couplings. The inverse phenomena (couplings shown with red arrows in (a)) can cause surface effects in flexoelectric models in finite samples. (b) and (c) depict the distribution of electric potential in a Lifshitz-invariant flexoelectric body without/with free surfaces.

$$\hat{\sigma}_{ij} = \frac{\partial \mathcal{H}}{\partial \varepsilon_{ij}} = \mathbf{C}_{ijkl} \varepsilon_{kl} + \zeta \mu_{lij} E_{l,k}, \quad (2)$$

$$\tilde{\sigma}_{ijk} = \frac{\partial \mathcal{H}}{\partial \varepsilon_{ij,k}} = h_{ijklmn} \varepsilon_{lm,n} - (1 - \zeta) \mu_{lij} E_l, \quad (3)$$

$$\hat{D}_l = -\frac{\partial \mathcal{H}}{\partial E_l} = \kappa_{lm} E_m + (1 - \zeta) \mu_{lij} \varepsilon_{ij,k}, \quad (4)$$

$$\tilde{D}_{ij} = -\frac{\partial \mathcal{H}}{\partial E_{i,j}} = M_{ijkl} E_{k,l} - \zeta \mu_{lij} \varepsilon_{kl}. \quad (5)$$

The physical stress and physical electric displacement are:

$$\sigma_{ij} = \frac{\partial \mathcal{H}}{\partial \varepsilon_{ij}} - \left(\frac{\partial \mathcal{H}}{\partial \varepsilon_{ij,k}} \right)_{,k} = \mathbf{C}_{ijkl} \varepsilon_{kl} + \mu_{lij} E_{l,k} - h_{ijklmn} \varepsilon_{lm,nk}, \quad (6)$$

and

$$D_i = \frac{\partial \mathcal{H}}{\partial E_i} - \left(\frac{\partial \mathcal{H}}{\partial E_{i,j}} \right)_{,j} = \kappa_{ij} E_j + \mu_{ijkl} \varepsilon_{jk,l} - M_{ijkl} E_{k,lj}. \quad (7)$$

The strong form of the problem can be written as:

$$\begin{cases} \sigma_{ij,j} + f_i^{ext} = 0 & \text{in } \Omega, \\ D_{l,l} - q = 0 & \text{in } \Omega, \end{cases} \quad (8)$$

where f_i^{ext} is the external body forces per unit volume, and q represents the external electric free charges per unit volume. The strong form is complemented with the following Neumann boundary conditions (Codony et al., 2021):

$$\left(\hat{\sigma}_{ij} - \tilde{\sigma}_{ijk,k} + \nabla_l^S(n_l) \tilde{\sigma}_{ijk} n_k \right) n_j - \nabla_j^S(\tilde{\sigma}_{ijk} n_k) = t_i \quad \text{on } \partial\Omega_t, \quad (9)$$

$$\tilde{\sigma}_{ijk} n_j n_k = r_i \quad \text{on } \partial\Omega_r, \quad (10)$$

$$-\left(\hat{D}_l - \tilde{D}_{lk,k} + \nabla_i^S(n_i) \tilde{D}_{lk} n_k \right) n_l + \nabla_l^S(\tilde{D}_{lk} n_k) = w \quad \text{on } \partial\Omega_w, \quad (11)$$

$$-\tilde{D}_{jk} n_j n_k = v \quad \text{on } \partial\Omega_v, \quad (12)$$

where \mathbf{n} is the normal vector to the surface, ∇^S denotes the surface divergence operator, \mathbf{t} is traction, \mathbf{r} is double traction, w is surface charge density, and v is double charge density. As discussed in Codony et al. (2021), in regions where the boundary is not smooth, some additional boundary conditions arise. However, this is not relevant to this study.

3. Analytical solutions for different cases

We provide next the analytical solution for three boundary value problems corresponding to a plane-strain microfilm under three loading conditions: axial electric actuation (Fig. 2a), axial compression (Fig. 2b), and uniform bending (Fig. 2c). For all the examples, we consider a thin flexoelectric film along the x -direction occupying $[-T/2, T/2]$ in the y -coordinate. The thin film is modeled as being infinite along x and z directions, for one-dimensional kinematics. For the described geometry, the boundary conditions presented in Eqs. (9)-(12) simplify to:

$$t_i = \sigma_{i2} \text{sign}(y) \quad \text{on } y = \pm T/2, \quad (13)$$

$$r_i = \tilde{\sigma}_{i22} \quad \text{on } y = \pm T/2, \quad (14)$$

$$w = -D_2 \text{sign}(y) \quad \text{on } y = \pm T/2, \quad (15)$$

$$v = -\tilde{D}_{22} \quad \text{on } y = \pm T/2. \quad (16)$$

Homogeneous Neumann mechanical and electric boundary conditions have been considered on the free surfaces for all the cases, i.e. $t_i = 0$, $r_i = 0$, $w = 0$, and $v = 0$. The obtained analytical results have been illustrated for each case considering a BST microfilm of thickness $T = 1$ micrometer. The material properties are given in Table 1. Worth noting that all analytical results have been verified against numerical simulations.

Table 1: BST material parameters used in this study.

E [Gpa]	ν	l_1 [nm]	ϵ [nC/Vm]	l_2 [nm]	μ_L [$\mu\text{C}/\text{m}$]	μ_T [$\mu\text{C}/\text{m}$]	μ_S [$\mu\text{C}/\text{m}$]
152	0.33	20	8	30	1.21	1.10	0.055

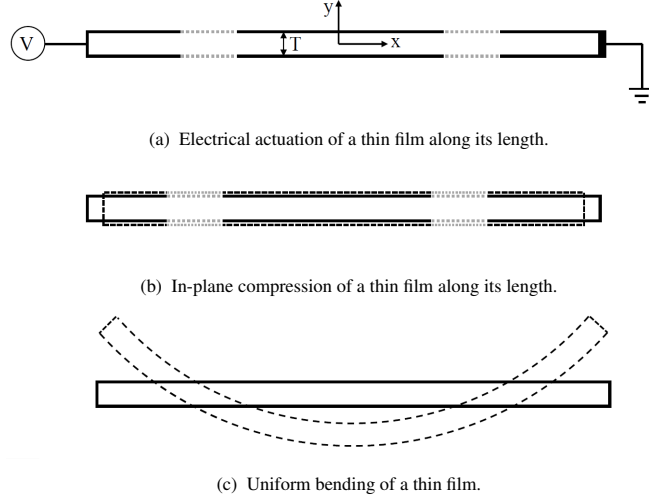


Figure 2: Loadings and boundary conditions of three cases studied in the paper. Dark dashed lines represent the deformed shape.

3.1. Axial electric actuation

Suppose we apply a far-field horizontal electric field \bar{E}_x to the system. Fig. 2a shows the boundary conditions and loadings for this case. Consequently, the applied electric field results in y -dependent shear strain $\varepsilon_{xy}(y) = \varepsilon_{yx}(y)$. Here we consider strain-free conditions at infinity so that $\varepsilon_{xx} = \varepsilon_{yy} = 0$ and $E_y = 0$. However, as shown in Appendix B, the stress $\sigma_{xx} = 0$ on each cross-section which implies that the conclusions are not affected by the choice of stress or strain-free boundary conditions at infinity. Therefore:

$$\boldsymbol{\varepsilon} = \begin{bmatrix} 0 & \varepsilon_{xy}(y) \\ \varepsilon_{xy}(y) & 0 \end{bmatrix}, \quad \mathbf{E} = \begin{bmatrix} \bar{E}_x \\ 0 \end{bmatrix}. \quad (17)$$

Considering homogeneous Neumann boundary conditions on the free surfaces, $\varepsilon_{xy}(y)$ can be obtained as:

$$\varepsilon_{xy}(y) = \frac{-(1 - \zeta)\mu_S \bar{E}_x}{(1 + \exp(-T/l_1)) C_S l_1} \left[\exp\left(\frac{-y - T/2}{l_1}\right) - \exp\left(\frac{y - T/2}{l_1}\right) \right]. \quad (18)$$

The details of the derivation of the solution are provided in Appendix B.

Fig. 3 depicts ε_{xy} along the cross-section, Eq. (18), for different flexoelectric models. It shows that for direct and Lifshitz-invariant models, as a result of the applied in-plane electric field, the top and bottom surfaces of the body experience shear strains. The shear strain vanishes at a certain distance from the surfaces. The profile of the shear strain is controlled by the strain gradient elasticity lengthscale l_1 and its magnitude is proportional to the applied electric field \bar{E}_x and the shear flexoelectric coefficient μ_S , and is inversely proportional to the shear component of the elasticity tensor C_S , and the strain gradient elasticity lengthscale l_1 . This behavior is similar to the actuation of a thin layer of a piezoelectric surface due to an application of external voltage, or inverse surface piezoelectricity. Fig. 3 shows that for this case, the converse model does not show surface effect.

3.2. Axial compression

Suppose we apply far-field plane-strain axial compression $\bar{\varepsilon}_{xx}$ to the body, Fig. 2b. Both the deformation field and electric potential are independent of the x -direction. Therefore, the applied compression results in y -dependent vertical strain $\varepsilon_{yy}(y)$ and electric field $E_y(y)$. Note that $\varepsilon_{xy} = \varepsilon_{yx} = 0$ and $E_x = 0$. Therefore:

$$\boldsymbol{\varepsilon} = \begin{bmatrix} \bar{\varepsilon}_{xx} & 0 \\ 0 & \varepsilon_{yy}(y) \end{bmatrix}, \quad \mathbf{E} = \begin{bmatrix} 0 \\ E_y(y) \end{bmatrix}. \quad (19)$$

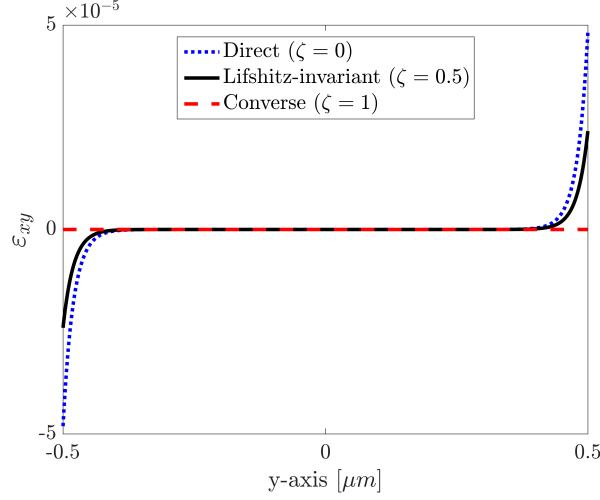


Figure 3: Electrical actuation of a thin flexoelectric film made of BST along its length with $\bar{E}_x = 1V/\mu m$ shows inverse surface piezoelectric-like effect.

Considering homogeneous Neumann boundary conditions on the free surfaces, $E_y(y)$ and $\varepsilon_{yy}(y)$ can be obtained with the following expressions:

$$E_y(y) = K \frac{\bar{\varepsilon}_{xx}(C_L \mu_T - C_T \mu_L)}{\epsilon C_L} \left[-\beta_2 \left[\exp\left(\frac{-y - T/2}{a_1}\right) - \exp\left(\frac{y - T/2}{a_1}\right) \right] + \beta_1 \left[\exp\left(\frac{-y - T/2}{a_2}\right) - \exp\left(\frac{y - T/2}{a_2}\right) \right] \right], \quad (20)$$

$$\varepsilon_{yy}(y) = K \frac{\bar{\varepsilon}_{xx}(C_L \mu_T - C_T \mu_L)}{\mu_L C_L} \left[-a_1 \alpha_1 \beta_2 \left[\exp\left(\frac{-y - T/2}{a_1}\right) + \exp\left(\frac{y - T/2}{a_1}\right) \right] + a_2 \alpha_2 \beta_1 \left[\exp\left(\frac{-y - T/2}{a_2}\right) + \exp\left(\frac{y - T/2}{a_2}\right) \right] \right] - \frac{C_T}{C_L} \bar{\varepsilon}_{xx}, \quad (21)$$

where

$$K = \frac{\zeta}{a_1 \beta_2 \gamma_1 - a_2 \beta_1 \gamma_2}, \quad (22)$$

$$a_1, a_2 = \sqrt{l_1 l_2} \sqrt{\frac{A}{1 \pm \sqrt{1 - A^2}}}, \quad A = \frac{2l_1 l_2}{l_1^2 + l_2^2 + l_\mu^2}, \quad (23)$$

$$l_\mu^2 = \frac{\mu_L^2}{C_L \epsilon}, \quad (24)$$

$$\alpha_i = 1 - \frac{l_2^2}{a_i^2}, \quad (25)$$

$$\beta_i = (1 - \exp(-T/a_i)) \left(\frac{l_1^2}{l_\mu^2} \alpha_i + 1 - \zeta \right), \quad (26)$$

$$\gamma_i = (1 + \exp(-T/a_i)) \left(\frac{l_2^2}{a_i^2} (1 - \zeta) + \zeta \right). \quad (27)$$

The details of the derivation of the solution are provided in [Appendix C](#). Note that in Eqs. (26), and (27), the thickness dependence of β_i and γ_i vanishes if $T \gg a_i$.

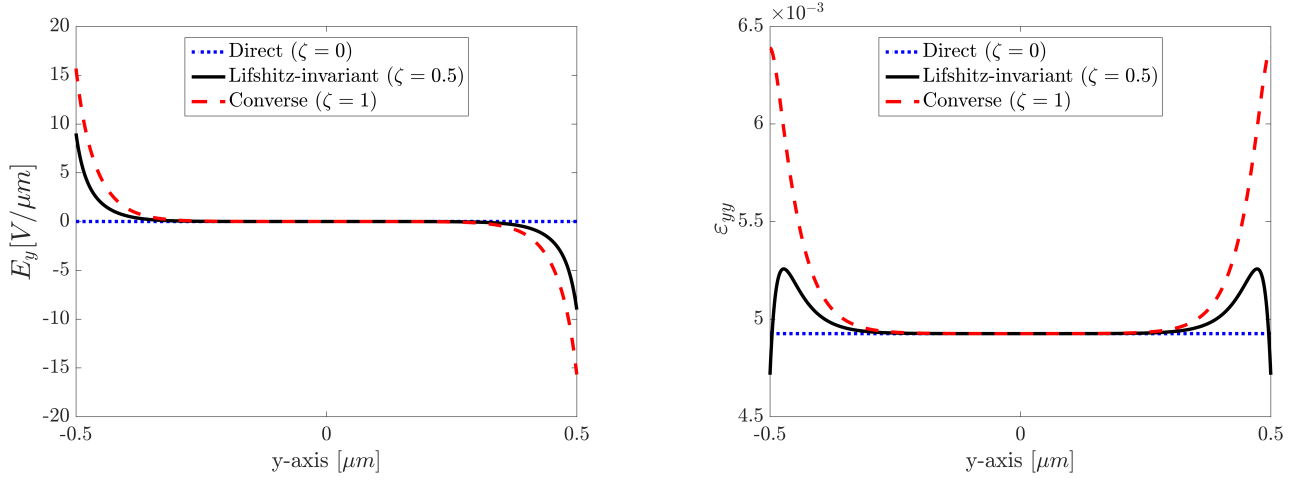


Figure 4: In-plane compression of a thin flexoelectric film made of BST along its length with $\bar{\epsilon}_{xx} = -0.01$ shows surface-piezoelectric like effect.

Fig. 4 depicts E_y and ϵ_{yy} along the cross-section, Eqs. (20) and (21), respectively, for different flexoelectric models. It shows that for Lifshitz-invariant and converse models, a boundary layer develops on the transversal electric field E_y , which vanishes away from the surface. This behavior is inherently similar to direct surface piezoelectricity in non-piezoelectric materials, where a thin layer of the surface shows an electric response under mechanical deformation. Due to the generated electric field gradient near the surfaces, the strain ϵ_{yy} also experiences a boundary layer due to converse flexoelectricity.

3.3. Uniform bending

Suppose the body is uniformly bent so that its curvature κ is the same in all cross-sections normal to it. Fig. 2c shows the boundary conditions and loadings for this case. Assuming slenderness, the strains and electric fields can be written as:

$$\boldsymbol{\epsilon} = \begin{bmatrix} -\kappa y & 0 \\ 0 & \epsilon_{yy}(y) \end{bmatrix}, \quad \mathbf{E} = \begin{bmatrix} 0 \\ E_y(y) \end{bmatrix}. \quad (28)$$

Considering homogeneous Neumann boundary conditions on the free surfaces, $E_y(y)$ and $\epsilon_{yy}(y)$ can be obtained with the following expressions:

$$E_y(y) = \frac{-\kappa(C_L\mu_T - C_T\mu_L)}{C_L\epsilon} \left[\hat{k}_1 \left[\exp\left(\frac{-y - T/2}{a_1}\right) + \exp\left(\frac{y - T/2}{a_1}\right) \right] - \hat{k}_2 \left[\exp\left(\frac{-y - T/2}{a_2}\right) + \exp\left(\frac{y - T/2}{a_2}\right) \right] \right] - \frac{\kappa}{\epsilon} \left(\mu_L \frac{C_T}{C_L} - \mu_T \right), \quad (29)$$

$$\epsilon_{yy}(y) = \frac{-\kappa(C_L\mu_T - C_T\mu_L)}{C_L\mu_L} \left[\hat{k}_5 \left[\exp\left(\frac{-y - T/2}{a_1}\right) - \exp\left(\frac{y - T/2}{a_1}\right) \right] - \hat{k}_6 \left[\exp\left(\frac{-y - T/2}{a_2}\right) - \exp\left(\frac{y - T/2}{a_2}\right) \right] \right] + \frac{C_T}{C_L} \kappa y, \quad (30)$$

where

$$\hat{k}_1 = \frac{(2a_2\hat{\gamma}_2(\zeta - 1) + \hat{\beta}_2 T\zeta)}{2(a_1\hat{\beta}_2\hat{\gamma}_1 - a_2\hat{\beta}_1\hat{\gamma}_2)}, \quad (31)$$

$$\hat{k}_2 = \frac{(2a_1\hat{\gamma}_1(\zeta - 1) + \hat{\beta}_1 T\zeta)}{2(a_1\hat{\beta}_2\hat{\gamma}_1 - a_2\hat{\beta}_1\hat{\gamma}_2)}, \quad (32)$$

$$\hat{k}_5 = \frac{a_1\alpha_1(2a_2\hat{\gamma}_2(\zeta - 1) + \hat{\beta}_2 T\zeta)}{2(a_1\hat{\beta}_2\hat{\gamma}_1 - a_2\hat{\beta}_1\hat{\gamma}_2)}, \quad (33)$$

$$\hat{k}_6 = \frac{a_2\alpha_2(2a_1\hat{\gamma}_1(\zeta - 1) + \hat{\beta}_1 T\zeta)}{2(a_1\hat{\beta}_2\hat{\gamma}_1 - a_2\hat{\beta}_1\hat{\gamma}_2)}, \quad (34)$$

$$\hat{\beta}_i = (1 + \exp(-T/a_i)) \left(\frac{l_\mu^2}{l_i^2} \alpha_i + 1 - \zeta \right), \quad (35)$$

$$\hat{\gamma}_i = (1 - \exp(-T/a_i)) \left(\frac{l_\mu^2}{a_i^2} (1 - \zeta) + \zeta \right). \quad (36)$$

where a_i , l_μ , and α_i have been defined in Eqs. (23)-(25). The details of the derivation of the solution have been provided in Appendix D. Note that in Eqs. (35), and (36), the thickness dependence of $\hat{\beta}_i$ and $\hat{\gamma}_i$ vanishes if $T \gg a_i$.

Fig. 5 depicts E_y and ε_{yy} along the cross-section, Eqs. (29) and (30), respectively, for different flexoelectric models. It is important to note that the surface effects seen in the case of bending are mainly a combination of the surface effects in the compression case, yet with opposite signs of the applied compression on two sides of the neutral axis. That is why the results shown in Fig. 5 exhibit an opposite symmetry compared to Fig. 4. Furthermore, the coupling between $\varepsilon_{yy,y}$ and E_y through μ_L causes an additional surface effect. That is why a small surface effect can be seen with the direct model in the case of bending.

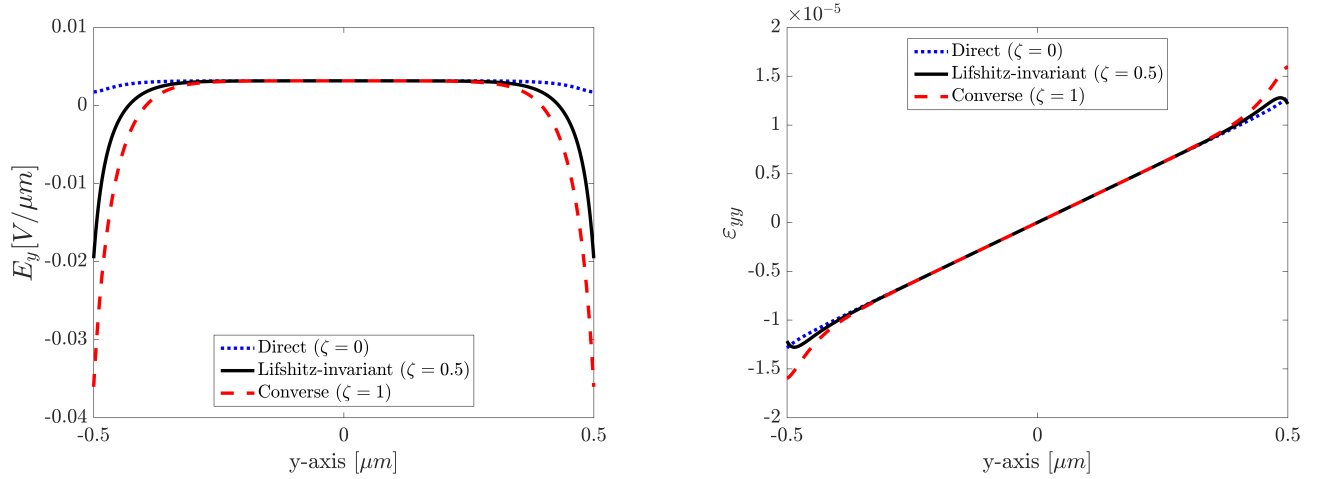


Figure 5: Surface effects of a flexoelectric thin film made of BST under uniform bending with $\kappa = 50[1/m]$.

3.4. Discussion

Three forms of coupling are mainly considered in the flexoelectric literature. Direct flexoelectricity is modeled as $-\mu_{lijk}\epsilon_{ijk}E_l$, converse flexoelectricity is modeled as $\mu_{lijk}\epsilon_{ij}E_{l,k}$, and Lifshitz-invariant flexoelectricity is modeled as $\frac{1}{2}\mu_{lijk}\epsilon_{ij}E_{l,k} - \frac{1}{2}\mu_{lijk}\epsilon_{ijk}E_l$. As shown in Section 2, considering any of the mentioned coupling terms explicitly in the

Table 2: The components of the strain or electric field that exhibit boundary layers for different cases and different flexoelectric models

Case	Direct ($\zeta = 0$)	Lifshitz-invariant ($\zeta = 0.5$)	Converse ($\zeta = 1$)
Electric actuation	ε_{xy}	ε_{xy}	-
Compression	-	ε_{yy}, E_y	ε_{yy}, E_y
Bending	ε_{yy}, E_y	ε_{yy}, E_y	ε_{yy}, E_y

electromechanical enthalpy would not change the governing equations, yet the definition of homogeneous Neumann boundary conditions is different in the three flexoelectric models. This results in solving different boundary value problems if the homogeneous Neumann boundary condition is imposed anywhere on the boundaries. Table 2 summarizes the components of the strain and electric field that exhibit boundary layers for the different case studies and different flexoelectric models. Electrical actuation and compression cases are of particular importance as the electromechanical response is isolated from the bulk flexoelectric response. As explained in Section 3.1, a homogeneous electric field can cause a shear strain gradient due to inverse flexoelectricity. This means that the surface of the body exhibits a mechanical response due to the application of an external electrical stimulus, or inverse surface piezoelectricity. Besides, as shown in Section 3.2, a homogeneous strain can cause an electric field gradient due to inverse converse flexoelectricity, a behavior that is similar to direct surface piezoelectricity. Considering either the direct or the converse flexoelectric models result in a one-way surface piezoelectric-like effect (direct or inverse), while the Lifshitz-invariant model shows a two-way surface piezoelectric-like effect (direct and inverse). The inherent surface effects of flexoelectricity with different models have already been seen in different studies (Yurkov and Tagantsev, 2016, Abdollahi et al., 2014, Zhuang et al., 2020, Codony et al., 2021). In particular, Codony et al. (2021) studied a cantilever beam under bending and showed that the Lifshitz-invariant model exhibits a boundary layer on E_y . This is in agreement with the results of this paper. However, as in Codony et al. (2021) the longitudinal flexoelectric coefficient μ_L was neglected, no boundary layer in E_y was observed in the direct model. The boundary layers have also been seen in a cantilever beam actuator (Abdollahi et al., 2014, He et al., 2019, Zhuang et al., 2020, Codony et al., 2021).

This analysis shed light on the origins of the surface effects in flexoelectric films, which for conciseness, have been considered in open-circuit conditions only. One could extend this analysis to short-circuited films by changing the boundary conditions (applying Dirichlet electric boundary conditions instead of homogeneous Neumann electric boundary conditions on free surfaces) to explain boundary layers present in that case.

3.5. Conclusions

In this work, we explored the continuum models of flexoelectricity in dielectrics. We showed that when the size of the body is finite, the continuum models of flexoelectricity in bulk exhibit surface piezoelectric-like effects. We attributed the surface effects to inverse flexoelectricity and inverse converse flexoelectricity. We showed that the direct and converse flexoelectric models exhibit a one-way surface piezoelectric-like effect, while the Lifshitz-invariant model shows a two-way surface piezoelectric-like effect. Furthermore, we characterized the observed boundary layers in terms of the lengthscales of the model. These findings may be critical in the design of sound one and two-dimensional analytical models for flexoelectric beams and films, which otherwise assume no boundary layers across the reduced dimension (Yan and Jiang, 2011, 2013, Codony et al., 2020, Chu et al., 2020, Wang et al., 2024, Mishra and Gupta, 2025, Shang et al., 2022), and may contribute overall in applications with an high surface to volume ratio, such as the development of lattice models for flexoelectric-metamaterials (Barceló-Mercader et al., 2024b, Greco et al., 2024).

Future research can be carried out to explore the interaction of the inherent surface effects of flexoelectricity with other physics (bulk piezoelectricity, surface piezoelectricity, and surface flexoelectricity). Besides, how to model flexoelectricity is still an open question (there is no clear physical understanding that which ζ parameter can well describe reality). There are also no clear insights into the high-order boundary conditions for which homogeneous Neumann conditions are commonly imposed in the literature for convenience. Furthermore, characterization of the physical lengthscales of the model still needs to be further researched. By comparing with other approaches (atomistic

simulations or experiments), the results provided here may be useful to find some of the parameters that are not yet well understood.

Acknowledgments

This work was supported by the Generalitat de Catalunya (“ICREA Academia” award for excellence in research to I.A., and Grants No. 2017-SGR-1278 and 2021-SGR-01049), the European Research Council (StG-679451 to I.A.), and the Spanish Ministry of Economy and Competitiveness (Grant PID2023-152533OB-I00 funded by MICIU/AEI/10.13039/501100011033/ERDF/EU, and Grant RTI2018-101662-B-I00). D.C. acknowledges the support of the Spanish Ministry of Universities through the Margarita Salas fellowship (European Union - NextGenerationEU). H.M. received the support of a fellowship from “la Caixa” Foundation (ID 100010434). The fellowship code is LCF/BQ/DI20/11780036. CIMNE is recipient of a Severo Ochoa Award of Excellence from the MINECO.

Appendix A. Material characterization

The electromechanical enthalpy density described in Eq. (1) involves five material tensors. We define them in this appendix. Below, the non-specified components of the material tensors are zero.

Isotropic elasticity tensor is considered here as

$$\begin{aligned} \mathbf{C}_{iiii} &= C_L, & i &= 1, 2, \\ \mathbf{C}_{iijj} &= C_T, & i, j &= 1, 2 \text{ with } i \neq j, \\ \mathbf{C}_{ijij} &= \mathbf{C}_{ijji} = C_S, & i, j &= 1, 2 \text{ with } i \neq j. \end{aligned} \quad (\text{A.1})$$

In plain strain condition, C_L, C_T and C_S are defined in terms of elasticity modulus Y and Poisson’s ratio ν as

$$C_L := \frac{Y(1-\nu)}{(1+\nu)(1-2\nu)}, \quad C_T := \frac{Y\nu}{(1+\nu)(1-2\nu)}, \quad C_S = \frac{C_L - C_T}{2} := \frac{Y}{2(1+\nu)}. \quad (\text{A.2})$$

We use a simplified form of isotropic strain elasticity tensor which depends on the elasticity modulus Y , the Poisson ratio ν and the internal length scale l_1 as (Mindlin, 1964, Altan and Aifantis, 1997)

$$\begin{aligned} h_{iikik} &= l_1^2 C_L, & i, k &= 1, 2, \\ h_{iikjk} &= l_1^2 C_T, & i, j, k &= 1, 2 \text{ with } i \neq j, \\ h_{ijkjk} &= h_{ijki} = l_1^2 C_S, & i, j, k &= 1, 2 \text{ with } i \neq j. \end{aligned} \quad (\text{A.3})$$

where the parameters C_L, C_S and C_T are defined in Eq. (A.2).

We use a second-order tensor to describe isotropic dielectricity κ , which depends on the electric permittivity ϵ as

$$\kappa_{ii} = \epsilon, \quad i = 1, 2. \quad (\text{A.4})$$

Flexoelectricity is represented by a fourth-order tensor μ . Ferroelectric perovskites in their paraelectric phase are characterized by a cubic-symmetric flexoelectricity tensor involving only three independent flexoelectric coefficients, namely longitudinal μ_L , transverse μ_T and shear μ_S .

$$\begin{aligned} \mu_{iiii} &= \mu_L, & i &= 1, 2, \\ \mu_{ijji} &= \mu_T, & i, j &= 1, 2 \text{ with } i \neq j, \\ \mu_{ijij} &= \mu_{ijji} = \mu_S, & i, j &= 1, 2 \text{ with } i \neq j. \end{aligned} \quad (\text{A.5})$$

We consider a simplified isotropic gradient dielectricity tensor which depends on electric permittivity of the material ϵ and the length scale ℓ_2 in the following form (Mindlin, 1968):

$$M_{ijij} = \epsilon \ell_2^2, \quad i, j = 1, 2. \quad (\text{A.6})$$

Appendix B. Analytical derivation for the case of electrical actuation of a thin flexoelectric film along its length

Consider a thin flexoelectric film along the x -direction occupying $[-T/2, T/2]$ in the y -coordinate. Suppose we apply far-field horizontal electric field \bar{E}_x to the system. Consequently, the applied electric field results in y -dependent shear strain $\varepsilon_{xy}(y) = \varepsilon_{yx}(y)$. Note that $\varepsilon_{xx} = \varepsilon_{yy} = 0$ and $E_y = 0$. Therefore:

$$\boldsymbol{\varepsilon} = \begin{bmatrix} 0 & \varepsilon_{xy}(y) \\ \varepsilon_{xy}(y) & 0 \end{bmatrix}, \quad \mathbf{E} = \begin{bmatrix} \bar{E}_x \\ 0 \end{bmatrix}. \quad (\text{B.1})$$

Accordingly, components of the constitutive equations can be written as:

$$\hat{\sigma}_{xy} = \hat{\sigma}_{yx} = 2C_S \varepsilon_{xy}(y), \quad (\text{B.2})$$

$$\hat{\sigma}_{xx} = \hat{\sigma}_{yy} = 0, \quad (\text{B.3})$$

$$\tilde{\sigma}_{xyy} = \tilde{\sigma}_{yyx} = 2C_S l_1^2 \varepsilon_{xy,y} - 2(1 - \zeta)\mu_S \bar{E}_x, \quad (\text{B.4})$$

$$\tilde{\sigma}_{xxx} = -(1 - \zeta)\mu_L \bar{E}_x, \quad (\text{B.5})$$

$$\tilde{\sigma}_{yyx} = -(1 - \zeta)\mu_T \bar{E}_x, \quad (\text{B.6})$$

$$\tilde{\sigma}_{yyy} = \tilde{\sigma}_{xyx} = \tilde{\sigma}_{yxx} = \tilde{\sigma}_{xxy} = 0, \quad (\text{B.7})$$

$$\hat{D}_x = \epsilon \bar{E}_x + 2(1 - \zeta)\mu_S \varepsilon_{xy,y}(y), \quad (\text{B.8})$$

$$\hat{D}_y = 0, \quad (\text{B.9})$$

$$\tilde{D}_{xy} = \tilde{D}_{yx} = -2\zeta\mu_S \varepsilon_{xy}(y), \quad (\text{B.10})$$

$$\tilde{D}_{xx} = \tilde{D}_{yy} = 0. \quad (\text{B.11})$$

Therefore, the components of physical stress and physical electric displacement are:

$$\sigma_{xy} = \sigma_{yx} = 2C_S \varepsilon_{xy}(y) - 2C_S l_1^2 \varepsilon_{xy,yy}(y), \quad (\text{B.12})$$

$$\sigma_{xx} = \sigma_{yy} = 0, \quad (\text{B.13})$$

$$D_x = \epsilon \bar{E}_x + 2\mu_S \varepsilon_{xy,y}(y) \quad (\text{B.14})$$

$$D_y = 0. \quad (\text{B.15})$$

Therefore, the following equilibrium equation in the y -direction is the only non-trivial equation that needs to be satisfied:

$$2C_S \varepsilon_{xy,y}(y) - 2l_1^2 C_S \varepsilon_{xy,yyy}(y) = 0, \quad (\text{B.16})$$

Note that the electrical equilibrium equation and its associated boundary conditions in the y -direction are trivially satisfied. The solution of the ODE (B.16) must then satisfy the following non-trivial boundary condition that is the homogeneous Neumann boundary condition related to double traction (Eq. (14)):

$$2l_1^2 C_S \varepsilon_{xy,y}(y) - 2(1 - \zeta)\mu_S \bar{E}_x = 0, \quad \text{on } y = \{-T/2, T/2\}. \quad (\text{B.17})$$

Note that the low-order mechanical boundary condition (Eq. (13)) in the y -direction is also trivially satisfied. The following is the solution for the above ODE (B.16) satisfying Eq. (B.17):

$$\varepsilon_{xy}(y) = \frac{-(1 - \zeta)\mu_S \bar{E}_x}{(1 + \exp(-T/l_1)) C_S l_1} \left[\exp\left(\frac{-y - T/2}{l_1}\right) - \exp\left(\frac{y - T/2}{l_1}\right) \right]. \quad (\text{B.18})$$

Appendix C. Analytical derivation for the case of in-plane compression of a thin flexoelectric film along its length

Consider a thin flexoelectric film along the x -direction occupying $[-T/2, T/2]$ in the y -coordinate. Suppose we apply far-field plane-strain horizontal compression $\bar{\varepsilon}_{xx}$ to the system. Both the deformation field and electric potential are independent of x -direction. Therefore, the applied compression results in y -dependent vertical strain $\varepsilon_{yy}(y)$ and electric field $E_y(y)$. Note that $\varepsilon_{xy} = \varepsilon_{yx} = 0$ and $E_x = 0$. Therefore:

$$\boldsymbol{\varepsilon} = \begin{bmatrix} \bar{\varepsilon}_{xx} & 0 \\ 0 & \varepsilon_{yy}(y) \end{bmatrix}, \quad \mathbf{E} = \begin{bmatrix} 0 \\ E_y(y) \end{bmatrix}. \quad (\text{C.1})$$

Accordingly, components of the constitutive equations can be written as:

$$\hat{\sigma}_{xx} = C_L \bar{\varepsilon}_{xx} + C_T \varepsilon_{yy}(y) + \zeta \mu_T E_{y,y}(y), \quad (\text{C.2})$$

$$\hat{\sigma}_{yy} = C_T \bar{\varepsilon}_{xx} + C_L \varepsilon_{yy}(y) + \zeta \mu_L E_{y,y}(y), \quad (\text{C.3})$$

$$\hat{\sigma}_{xy} = \hat{\sigma}_{yx} = 0, \quad (\text{C.4})$$

$$\bar{\sigma}_{yyy} = l_1^2 C_L \varepsilon_{yy,y}(y) - (1 - \zeta) \mu_L E_y(y), \quad (\text{C.5})$$

$$\bar{\sigma}_{xyx} = \bar{\sigma}_{yxx} = -(1 - \zeta) \mu_S E_y(y), \quad (\text{C.6})$$

$$\bar{\sigma}_{xxy} = l_1^2 C_T \varepsilon_{yy,y}(y) - (1 - \zeta) \mu_T E_y(y), \quad (\text{C.7})$$

$$\bar{\sigma}_{xxx} = \bar{\sigma}_{xyy} = \bar{\sigma}_{yyx} = \bar{\sigma}_{yxy} = 0, \quad (\text{C.8})$$

$$\hat{D}_y = \varepsilon E_y(y) + (1 - \zeta) \mu_L \varepsilon_{yy,y}(y), \quad (\text{C.9})$$

$$\hat{D}_x = 0, \quad (\text{C.10})$$

$$\bar{D}_{xx} = -\zeta \mu_L \bar{\varepsilon}_{xx} - \zeta \mu_T \varepsilon_{yy}(y), \quad (\text{C.11})$$

$$\bar{D}_{yy} = l_2^2 \varepsilon E_{y,y}(y) - \zeta \mu_L \varepsilon_{yy}(y) - \zeta \mu_T \bar{\varepsilon}_{xx}, \quad (\text{C.12})$$

$$\bar{D}_{xy} = \bar{D}_{yx} = 0. \quad (\text{C.13})$$

Therefore, the components of physical stress and physical electric displacement are:

$$\sigma_{xx} = C_L \bar{\varepsilon}_{xx} + C_T \varepsilon_{yy}(y) + \mu_T E_{y,y}(y) - l_1^2 C_T \varepsilon_{yy,y}(y), \quad (\text{C.14})$$

$$\sigma_{yy} = C_T \bar{\varepsilon}_{xx} + C_L \varepsilon_{yy}(y) + \mu_L E_{y,y}(y) - l_1^2 C_L \varepsilon_{yy,y}(y), \quad (\text{C.15})$$

$$\sigma_{xy} = \sigma_{yx} = 0, \quad (\text{C.16})$$

$$D_y = \varepsilon E_y(y) + \mu_L \varepsilon_{yy,y}(y) - l_2^2 \varepsilon E_{y,y}(y), \quad (\text{C.17})$$

$$D_x = 0. \quad (\text{C.18})$$

Therefore, equilibrium equations in y -direction read:

$$C_L \varepsilon_{yy,y}(y) + \mu_L E_{y,y}(y) - l_1^2 C_L \varepsilon_{yy,yyy}(y) = 0, \quad (\text{C.19})$$

$$\varepsilon E_{y,y}(y) + \mu_L \varepsilon_{yy,y}(y) - l_2^2 \varepsilon E_{y,yyy}(y) = 0, \quad (\text{C.20})$$

subjected to high-order homogeneous Neumann boundary conditions (Eqs. (14), (16)):

$$l_1^2 C_L \varepsilon_{yy,y}(y) - (1 - \zeta) \mu_L E_y(y) = 0, \quad \text{on } y = \{-T/2, T/2\}, \quad (\text{C.21})$$

$$l_2^2 \varepsilon E_{y,y}(y) - \zeta \mu_L \varepsilon_{yy}(y) - \zeta \mu_T \bar{\varepsilon}_{xx} = 0, \quad \text{on } y = \{-T/2, T/2\}. \quad (\text{C.22})$$

The low-order homogeneous Neumann boundary conditions (Eqs. (13),(15)) will naturally be satisfied with the solution we will postulate.

Extracting $E_{y,y}$ and $\varepsilon_{yy,y}$ from (C.15) and (C.17), respectively, and replacing them into (C.19) and (C.20), respectively, we obtain:

$$(l_1^2 l_2^2) E_{y,yyy}(y) - (l_1^2 + l_2^2 + l_\mu^2) E_{y,yy}(y) + E_y(y) = \frac{D_y - l_1^2 D_{y,yy}}{\epsilon}, \quad (\text{C.23})$$

$$(l_1^2 l_2^2) \varepsilon_{yy,yyy}(y) - (l_1^2 + l_2^2 + l_\mu^2) \varepsilon_{yy,yy}(y) + \varepsilon_{yy}(y) = \frac{\sigma_{yy} - l_2^2 \sigma_{yy,yy}}{C_L} - \frac{C_T}{C_L} \bar{\varepsilon}_{xx}, \quad (\text{C.24})$$

where $l_\mu^2 = \frac{\mu_i^2}{C_L \epsilon}$.

One can postulate the solutions to be of the form:

$$E_y = k_1 \exp\left(\frac{-y - T/2}{a_1}\right) + k_2 \exp\left(\frac{-y - T/2}{a_2}\right) + k_3 \exp\left(\frac{y - T/2}{a_1}\right) + k_4 \exp\left(\frac{y - T/2}{a_2}\right), \quad (\text{C.25})$$

$$\varepsilon_{yy}(y) = k_5 \exp\left(\frac{-y - T/2}{a_1}\right) + k_6 \exp\left(\frac{-y - T/2}{a_2}\right) + k_7 \exp\left(\frac{y - T/2}{a_1}\right) + k_8 \exp\left(\frac{y - T/2}{a_2}\right) - \frac{C_T}{C_L} \bar{\varepsilon}_{xx}, \quad (\text{C.26})$$

for $y \in [-T/2, T/2]$, with:

$$a_1, a_2 = \sqrt{\frac{2l_1^2 l_2^2}{l_1^2 + l_2^2 + l_\mu^2 \pm \sqrt{(l_1^2 + l_2^2 + l_\mu^2)^2 - 4l_1^2 l_2^2}}}. \quad (\text{C.27})$$

Note that $k_1 = -k_3$, $k_2 = -k_4$, $k_5 = k_7$, $k_6 = k_8$ due to symmetry. Substituting the E_y and ε_{yy} from Eqs. (C.25) and (C.26) to Eqs. (C.19), (C.20), (C.21) and (C.22), we obtain the unknowns k_i .

$$k_1 = -k_3 = \frac{-\beta_2 \bar{\varepsilon}_{xx} \zeta (C_L \mu_T - C_T \mu_L)}{C_L \epsilon (a_1 \beta_2 \gamma_1 - a_2 \beta_1 \gamma_2)}, \quad (\text{C.28})$$

$$k_2 = -k_4 = \frac{\beta_1 \bar{\varepsilon}_{xx} \zeta (C_L \mu_T - C_T \mu_L)}{C_L \epsilon (a_1 \beta_2 \gamma_1 - a_2 \beta_1 \gamma_2)}, \quad (\text{C.29})$$

$$k_5 = k_7 = \frac{-a_1 \alpha_1 \beta_2 \bar{\varepsilon}_{xx} \zeta (C_L \mu_T - C_T \mu_L)}{C_L \mu_L (a_1 \beta_2 \gamma_1 - a_2 \beta_1 \gamma_2)}, \quad (\text{C.30})$$

$$k_6 = k_8 = \frac{a_2 \alpha_2 \beta_1 \bar{\varepsilon}_{xx} \zeta (C_L \mu_T - C_T \mu_L)}{C_L \mu_L (a_1 \beta_2 \gamma_1 - a_2 \beta_1 \gamma_2)}, \quad (\text{C.31})$$

where

$$\alpha_i = 1 - \frac{l_2^2}{a_i^2}, \quad (\text{C.32})$$

$$\beta_i = (1 - \exp(-T/a_i)) \left(\frac{l_1^2}{l_\mu^2} \alpha_i + 1 - \zeta \right), \quad (\text{C.33})$$

$$\gamma_i = (1 + \exp(-T/a_i)) \left(\frac{l_2^2}{a_i^2} (1 - \zeta) + \zeta \right). \quad (\text{C.34})$$

Appendix D. Analytical derivation for the case of uniform bending of a slender beam

Consider thin flexoelectric film along the x -direction occupying $[-T/2, T/2]$ in the y -coordinate. It is uniformly bent so that its curvature κ is the same in all cross-sections normal to it. Assuming slenderness, the strains and electric fields can be written as:

$$\boldsymbol{\varepsilon} = \begin{bmatrix} -\kappa y & 0 \\ 0 & \varepsilon_{yy}(y) \end{bmatrix}, \quad \mathbf{E} = \begin{bmatrix} 0 \\ E_y(y) \end{bmatrix}. \quad (\text{D.1})$$

Accordingly, components of the constitutive equations can be written as:

$$\hat{\sigma}_{xx} = -C_L \kappa y + C_T \varepsilon_{yy}(y) + \zeta \mu_T E_{y,y}(y), \quad (\text{D.2})$$

$$\hat{\sigma}_{yy} = -C_T \kappa y + C_L \varepsilon_{yy}(y) + \zeta \mu_L E_{y,y}(y), \quad (\text{D.3})$$

$$\hat{\sigma}_{xy} = \hat{\sigma}_{yx} = 0, \quad (\text{D.4})$$

$$\tilde{\sigma}_{yyy} = l_1^2 C_L \varepsilon_{yy,y}(y) - (1 - \zeta) \mu_L E_y(y) - l_1^2 C_T \kappa, \quad (\text{D.5})$$

$$\tilde{\sigma}_{xyx} = \tilde{\sigma}_{yxx} = -(1 - \zeta) \mu_S E_y(y), \quad (\text{D.6})$$

$$\tilde{\sigma}_{xxy} = l_1^2 C_T \varepsilon_{yy,y}(y) - (1 - \zeta) \mu_T E_y(y) - l_1^2 C_L \kappa, \quad (\text{D.7})$$

$$\tilde{\sigma}_{xxx} = \tilde{\sigma}_{xyy} = \tilde{\sigma}_{yyx} = \tilde{\sigma}_{yxy} = 0, \quad (\text{D.8})$$

$$\hat{D}_y = \epsilon E_y(y) + (1 - \zeta) \mu_L \varepsilon_{yy,y}(y) - (1 - \zeta) \mu_T \kappa, \quad (\text{D.9})$$

$$\hat{D}_x = 0, \quad (\text{D.10})$$

$$\tilde{D}_{xx} = \zeta \mu_L \kappa y - \zeta \mu_T \varepsilon_{yy}(y), \quad (\text{D.11})$$

$$\tilde{D}_{yy} = l_2^2 \epsilon E_{y,y}(y) - \zeta \mu_L \varepsilon_{yy}(y) + \zeta \mu_T \kappa y, \quad (\text{D.12})$$

$$\tilde{D}_{xy} = \tilde{D}_{yx} = 0. \quad (\text{D.13})$$

Therefore, the components of physical stress and physical electric displacement are:

$$\sigma_{xx} = -C_L \kappa y + C_T \varepsilon_{yy}(y) + \mu_T E_{y,y}(y) - l_1^2 C_T \varepsilon_{yy,yy}(y), \quad (\text{D.14})$$

$$\sigma_{yy} = -C_T \kappa y + C_L \varepsilon_{yy}(y) + \mu_L E_{y,y}(y) - l_1^2 C_L \varepsilon_{yy,yy}(y), \quad (\text{D.15})$$

$$\sigma_{xy} = \sigma_{yx} = 0, \quad (\text{D.16})$$

$$D_y = \epsilon E_y(y) + \mu_L \varepsilon_{yy,y}(y) - \mu_T \kappa - l_2^2 \epsilon E_{y,yy}(y), \quad (\text{D.17})$$

$$D_x = 0. \quad (\text{D.18})$$

Therefore, equilibrium equations in y-direction read:

$$-C_T \kappa + C_L \varepsilon_{yy,y}(y) + \mu_L E_{y,yy}(y) - l_1^2 C_L \varepsilon_{yy,yyy}(y) = 0, \quad (\text{D.19})$$

$$\epsilon E_{y,y}(y) + \mu_L \varepsilon_{yy,yy}(y) - l_2^2 \epsilon E_{y,yyy}(y) = 0, \quad (\text{D.20})$$

subjected to homogeneous Neumann boundary conditions (Eqs. (14),(16)):

$$l_1^2 C_L \varepsilon_{yy,y}(y) - (1 - \zeta) \mu_L E_y(y) - l_1^2 C_T \kappa = 0, \quad \text{on } y = \{-\frac{T}{2}, \frac{T}{2}\}, \quad (\text{D.21})$$

$$l_2^2 \epsilon E_{y,y}(y) - \zeta \mu_L \varepsilon_{yy}(y) + \zeta \mu_T \kappa y = 0, \quad \text{on } y = \{-\frac{T}{2}, \frac{T}{2}\}. \quad (\text{D.22})$$

The low-order homogeneous Neumann boundary conditions (Eqs. (13),(15)) will be satisfied with the solution we will postulate.

Extracting $E_{y,y}$ and $\varepsilon_{yy,y}$ from (D.15) and (D.17), respectively, and replacing them into (D.19) and (D.20), respectively, we obtain:

$$(l_1^2 l_2^2) E_{y,yyy}(y) - (l_1^2 + l_2^2 + l_\mu^2) E_{y,yy}(y) + E_y(y) = \frac{D_y - l_1^2 D_{y,yy}}{\epsilon} - \frac{\kappa}{\epsilon} (\mu_L \frac{C_T}{C_L} - \mu_T), \quad (\text{D.23})$$

$$(l_1^2 l_2^2) \varepsilon_{yy,yyy}(y) - (l_1^2 + l_2^2 + l_\mu^2) \varepsilon_{yy,yy}(y) + \varepsilon_{yy}(y) = \frac{\sigma_{yy} - l_2^2 \sigma_{yy,yy}}{C_L} + \frac{C_T}{C_L} \kappa y. \quad (\text{D.24})$$

where $l_\mu^2 = \frac{\mu_L^2}{C_L \epsilon}$.

One can postulate the solutions to be of the form:

$$E_y = k_1 \exp\left(\frac{-y - T/2}{a_1}\right) + k_2 \exp\left(\frac{-y - T/2}{a_2}\right) + k_3 \exp\left(\frac{y - T/2}{a_1}\right) + k_4 \exp\left(\frac{y - T/2}{a_2}\right) - \frac{\kappa}{\epsilon} \left(\mu_L \frac{C_T}{C_L} - \mu_T \right), \quad (\text{D.25})$$

$$\varepsilon_{yy}(y) = k_5 \exp\left(\frac{-y - T/2}{a_1}\right) + k_6 \exp\left(\frac{-y - T/2}{a_2}\right) + k_7 \exp\left(\frac{y - T/2}{a_1}\right) + k_8 \exp\left(\frac{y - T/2}{a_2}\right) + \frac{C_T}{C_L} \kappa y, \quad (\text{D.26})$$

for $y \in [-T/2, T/2]$, with:

$$a_1, a_2 = \sqrt{\frac{2l_1^2 l_2^2}{l_1^2 + l_2^2 + l_\mu^2 \pm \sqrt{(l_1^2 + l_2^2 + l_\mu^2)^2 - 4l_1^2 l_2^2}}}. \quad (\text{D.27})$$

Note that $k_1 = k_3$, $k_2 = k_4$, $k_5 = -k_7$, $k_6 = -k_8$ due to symmetry. Substituting the E_y and ε_{yy} from Eqs. (D.25) and (D.26) to Eqs. (D.19), (D.20), (D.21) and (D.22), we obtain the unknowns k_i .

$$k_1 = k_3 = \frac{-\kappa(C_L \mu_T - C_T \mu_L)(2a_2 \hat{\gamma}_2(\zeta - 1) + \hat{\beta}_2 T \zeta)}{2C_L \epsilon (a_1 \hat{\beta}_2 \hat{\gamma}_1 - a_2 \hat{\beta}_1 \hat{\gamma}_2)}, \quad (\text{D.28})$$

$$k_2 = k_4 = \frac{\kappa(C_L \mu_T - C_T \mu_L)(2a_1 \hat{\gamma}_1(\zeta - 1) + \hat{\beta}_1 T \zeta)}{2C_L \epsilon (a_1 \hat{\beta}_2 \hat{\gamma}_1 - a_2 \hat{\beta}_1 \hat{\gamma}_2)}, \quad (\text{D.29})$$

$$k_5 = -k_7 = \frac{-a_1 \alpha_1 \kappa (C_L \mu_T - C_T \mu_L)(2a_2 \hat{\gamma}_2(\zeta - 1) + \hat{\beta}_2 T \zeta)}{2C_L \mu_L (a_1 \hat{\beta}_2 \hat{\gamma}_1 - a_2 \hat{\beta}_1 \hat{\gamma}_2)}, \quad (\text{D.30})$$

$$k_6 = -k_8 = \frac{a_2 \alpha_2 \kappa (C_L \mu_T - C_T \mu_L)(2a_1 \hat{\gamma}_1(\zeta - 1) + \hat{\beta}_1 T \zeta)}{2C_L \mu_L (a_1 \hat{\beta}_2 \hat{\gamma}_1 - a_2 \hat{\beta}_1 \hat{\gamma}_2)}. \quad (\text{D.31})$$

where

$$\alpha_i = 1 - \frac{l_2^2}{a_i^2}, \quad (\text{D.32})$$

$$\hat{\beta}_i = (1 + \exp(-T/a_i)) \left(\frac{l_2^2}{l_\mu^2} \alpha_i + 1 - \zeta \right), \quad (\text{D.33})$$

$$\hat{\gamma}_i = (1 - \exp(-T/a_i)) \left(\frac{l_2^2}{a_i^2} (1 - \zeta) + \zeta \right). \quad (\text{D.34})$$

References

- A. Abdollahi, D. Millán, C. Peco, M. Arroyo, and I. Arias. Revisiting pyramid compression to quantify flexoelectricity: A three-dimensional simulation study. *Phys. Rev. B*, 91:104103, Mar 2015. URL <http://dx.doi.org/10.1103/PhysRevB.91.104103>.
- Amir Abdollahi, Christian Peco, Daniel Millan, Marino Arroyo, and Irene Arias. Computational evaluation of the flexoelectric effect in dielectric solids. *Journal of Applied Physics*, 116(9):93502, 2014.
- Amir Abdollahi, Neus Domingo, Irene Arias, and Gustau Catalan. Converse flexoelectricity yields large piezoresponse force microscopy signals in non-piezoelectric materials. *Nature communications*, 10(1):1–6, 2019.
- Fatemeh Ahmadpoor and Pradeep Sharma. Flexoelectricity in two-dimensional crystalline and biological membranes. *Nanoscale*, 7(40):16555–16570, 2015.
- B S Altan and E C Aifantis. On some aspects in the special theory of gradient elasticity. *Journal of the Mechanical Behavior of Materials*, 8(3): 231–282, 1997.
- Jordi Barceló-Mercader, David Codony, Sonia Fernández-Méndez, and Irene Arias. Weak enforcement of interface continuity and generalized periodicity in high-order electromechanical problems. *International Journal for Numerical Methods in Engineering*, 123(4):901–923, 2022.
- Jordi Barceló-Mercader, David Codony, Alice Mocchi, and Irene Arias. Computational homogenization of higher-order electro-mechanical materials with built-in generalized periodicity conditions. *Computer Methods in Applied Mechanics and Engineering*, 423:116861, 2024a.
- Jordi Barceló-Mercader, David Codony, Alice Mocchi, and Irene Arias. Computational homogenization of higher-order electro-mechanical materials with built-in generalized periodicity conditions. *Computer Methods in Applied Mechanics and Engineering*, 423:116861, 2024b.

- Umesh Kumar Bhaskar, Nirupam Banerjee, Amir Abdollahi, Zhe Wang, Darrell G Schlom, Guus Rijnders, and Gustau Catalan. A flexoelectric microelectromechanical system on silicon. *Nature nanotechnology*, 11(3):263–266, 2016.
- J M Bursian and O I Zaikovskii. Changes in curvature of a ferroelectric film due to polarization. *Soviet Physics Solid State*, 10(5):1121–1124, 1968.
- Liangliang Chu, Yanbin Li, and Guansuo Dui. Nonlinear analysis of functionally graded flexoelectric nanoscale energy harvesters. *International Journal of Mechanical Sciences*, 167:105282, 2020. ISSN 0020-7403. doi: <https://doi.org/10.1016/j.ijmecsci.2019.105282>. URL <https://www.sciencedirect.com/science/article/pii/S0020740319325779>.
- D Codony, Alice Mocci, Jordi Barceló-Mercader, and I Arias. Mathematical and computational modeling of flexoelectricity. *Journal of Applied Physics*, 130(23):231102, 2021.
- David Codony, Onofre Marco, Sonia Fernández-Méndez, and Irene Arias. An Immersed Boundary Hierarchical B-spline method for flexoelectricity. *Computer Methods in Applied Mechanics and Engineering*, 2019.
- David Codony, Prakhar Gupta, Onofre Marco, and Irene Arias. Modeling flexoelectricity in soft dielectrics at finite deformation. *Journal of the Mechanics and Physics of Solids*, page 104182, 2020.
- L Eric Cross. Flexoelectric effects: Charge separation in insulating solids subjected to elastic strain gradients. *Journal of Materials Science*, 41: 53–63, 2006.
- Shuangxing Dai, Mohamed Gharbi, Pradeep Sharma, and Harold S Park. Surface piezoelectricity: size effects in nanostructures and the emergence of piezoelectricity in non-piezoelectric materials. *Journal of Applied Physics*, 110(10):104305, 2011.
- Alexandre Danescu. Hyper-pre-stress vs. strain-gradient for surface relaxation in diamond-like structures. *Journal of the Mechanics and Physics of Solids*, 60(4):623–642, 2012.
- Francesco Greco, David Codony, Hossein Mohammadi, Sonia Fernandez-Mendez, and Irene Arias. Topology optimization of flexoelectric metamaterials with apparent piezoelectricity. *Journal of the Mechanics and Physics of Solids*, 183:105477, 2024.
- Bo He, Brahmanandam Javvaji, and Xiaoying Zhuang. Characterizing flexoelectricity in composite material using the element-free Galerkin method. *Energies*, 12(2):271, 2019.
- David CC Lam, Fan Yang, ACM Chong, Jianxun Wang, and Pin Tong. Experiments and theory in strain gradient elasticity. *Journal of the Mechanics and Physics of Solids*, 51(8):1477–1508, 2003.
- Haidong Lu, C-W Bark, D Esque De Los Ojos, J Alcalá, Chang-Beom Eom, G Catalan, and Alexei Gruverman. Mechanical writing of ferroelectric polarization. *Science*, 336(6077):59–61, 2012. URL <https://doi.org/10.1126/science.1218693>.
- Wenhui Ma and L Eric Cross. Observation of the flexoelectric effect in relaxor Pb (Mg $_{1/3}$ Nb $_{2/3}$) O₃ ceramics. *Appl. Phys. Lett.*, 78(19): 2920–2921, 2001. URL <https://doi.org/10.1063/1.1356444>.
- Wenhui Ma and L Eric Cross. Flexoelectric polarization of barium strontium titanate in the paraelectric state. *Applied Physics Letters*, 81(18): 3440–3442, 2002.
- VS Mashkevich and KB Tolpygo. Electrical, optical and elastic properties of diamond type crystals. *Sov. Phys. JETP*, 5(3):435–439, 1957.
- Raymond David Mindlin. Micro-structure in linear elasticity. *Archive for Rational Mechanics and Analysis*, 16(1):51–78, 1964.
- Raymond David Mindlin. Polarization gradient in elastic dielectrics. *International Journal of Solids and Structures*, 4(6):637–642, 1968. doi: 10.1016/0020-7683(68)90079-6. URL [http://dx.doi.org/10.1016/0020-7683\(68\)90079-6](http://dx.doi.org/10.1016/0020-7683(68)90079-6).
- Pushkar Mishra and Prakhar Gupta. Modeling direct and converse flexoelectricity in soft dielectric rods with application to the follower load. *Journal of the Mechanics and Physics of Solids*, 195:105956, 2025.
- Thanh D Nguyen, Sheng Mao, Yao-Wen Yeh, Prashant K Purohit, and Michael C McAlpine. Nanoscale flexoelectricity. *Advanced Materials*, 25(7):946–974, 2013.
- XiaHui Pan, ShouWen Yu, and XiQiao Feng. A continuum theory of surface piezoelectricity for nanodielectrics. *Science China Physics, Mechanics and Astronomy*, 54(4):564–573, 2011.
- Hongxing Shang, Xu Liang, Feng Deng, Shuling Hu, and Shengping Shen. Flexoelectricity in wrinkled thin films. *International Journal of Mechanical Sciences*, 234:107685, 2022.
- P Sharma, S Ryu, JD Burton, TR Paudel, CW Bark, Z Huang, EY Tsybmal, G Catalan, CB Eom, and A Gruverman. Mechanical tuning of laalo3/srtio3 interface conductivity. *Nano letters*, 15(5):3547–3551, 2015.
- HM SHODJA, F AHMADPOOR, and A TEHRANCHI. Calculation of the additional constants for fcc materials in second strain gradient elasticity behavior of a nano-size bernoulli-euler beam with surface effects. *Journal of applied mechanics*, 79(2), 2012.
- John Y Shu, Wayne E King, and Norman A Fleck. Finite elements for materials with strain gradient effects. *International Journal for Numerical Methods in Engineering*, 44(3):373–391, 1999.
- Alexander K Tagantsev and Alexander S Yurkov. Flexoelectric effect in finite samples. *Journal of Applied Physics*, 112(4):44103, 2012. doi: 10.1063/1.4745037. URL <http://dx.doi.org/10.1063/1.4745037>.
- Bo Wang, Yijia Gu, Shujun Zhang, and Long-Qing Chen. Flexoelectricity in solids: Progress, challenges, and perspectives. *Progress in Materials Science*, 106:100570, 2019. ISSN 0079-6425. doi: <https://doi.org/10.1016/j.pmatsci.2019.05.003>. URL <http://www.sciencedirect.com/science/article/pii/S0079642519300465>.
- Peng Wang, JiaWei Xu, XiWen Zhang, and YingHui Lv. Free vibration of nanobeams with surface and dynamic flexoelectric effects. *Scientific Reports*, 14(1):1–12, 2024.
- Z Yan and LY Jiang. Flexoelectric effect on the electroelastic responses of bending piezoelectric nanobeams. *Journal of Applied Physics*, 113(19), 2013.
- Zhi Yan and Liying Jiang. Surface effects on the electromechanical coupling and bending behaviours of piezoelectric nanowires. *Journal of Physics D: Applied Physics*, 44(7):075404, 2011.
- Ming-Min Yang, Dong Jik Kim, and Marin Alexe. Flexo-photovoltaic effect. *Science*, 360(6391):904–907, 2018.
- P V Yudin and A K Tagantsev. Fundamentals of flexoelectricity in solids. *Nanotechnology*, 24(43):432001, 2013. URL <http://stacks.iop.org/0957-4484/24/i=43/a=432001>.
- A S Yurkov and A K Tagantsev. Strong surface effect on direct bulk flexoelectric response in solids. *Appl. Phys. Lett.*, 108(2):22904, 2016. URL <https://doi.org/10.1063/1.4939975>.

Julien Yvonnet and LP1439 Liu. A numerical framework for modeling flexoelectricity and maxwell stress in soft dielectrics at finite strains. *Computer Methods in Applied Mechanics and Engineering*, 313:450–482, 2017.

Xiaoying Zhuang, Binh Huy Nguyen, Subbiah Srivilliputtur Nanthakumar, Thai Quoc Tran, Naif Alajlan, and Timon Rabczuk. Computational Modeling of Flexoelectricity—A Review. *Energies*, 13(6):1326, 2020.

Pavlo Zubko, Gustau Catalan, and Alexander K Tagantsev. Flexoelectric effect in solids. *Annual Review of Materials Research*, 43, 2013.